

OPEN

# First Experience With a Whole-Body Spectral Photon-Counting CT Clinical Prototype

Salim A. Si-Mohamed, MD, PhD,\*† Sara Boccacini, MD, PhD,\*† Marjorie Villien, PhD,‡ Yoad Yagil, PhD,§ Klaus Erhard, PhD,|| Loic Bousset, MD, PhD,\*† and Philippe C. Douek, MD, PhD\*†

**Abstract:** Spectral photon-counting computed tomography (SPCCT) technology holds great promise for becoming the next generation of computed tomography (CT) systems. Its technical characteristics have many advantages over conventional CT imaging. For example, SPCCT provides better spatial resolution, greater dose efficiency for ultra-low-dose and low-dose protocols, and tissue contrast superior to that of conventional CT. In addition, SPCCT takes advantage of several known approaches in the field of spectral CT imaging, such as virtual monochromatic imaging and material decomposition imaging. In addition, SPCCT takes advantage of a new approach in this field, known as K-edge imaging, which allows specific and quantitative imaging of a heavy atom-based contrast agent. Hence, the high potential of SPCCT systems supports their ongoing investigation in clinical research settings. In this review, we propose an overview of our clinical research experience of a whole-body SPCCT clinical prototype, to give an insight into the potential benefits for clinical human imaging on image quality, diagnostic confidence, and new approaches in spectral CT imaging.

**Key Words:** computed tomography, spectral photon-counting CT, spectral CT, cardiovascular, chest: Human

(*Invest Radiol* 2023;58: 459–471)

The recent introduction of spectral photon-counting computed tomography (SPCCT) technology in routine clinical practice marks a turning point in the field of medical imaging. It illustrates the successful translation of a ground-breaking innovation, from bench to bedside, at the service of Medicine. This innovation, based on photon-counting detectors, has the potential to improve the overall performance of current computed tomography (CT) systems by increasing spatial resolution and reducing noise, beam hardening, and x-ray doses among other things. Spectral photon-counting CT also provides the opportunity to explore new approaches that were previously unavailable in the field of CT, such as molecular, functional imaging. However, like any innovation, it will need to be fully adopted by the radiology community to evaluate its added clinical relevance and validate its daily use with respect to

potential impediments related to workflow, data management, and slow adoption of a new tool.

In this review, we propose an overview of our clinical research experience of a whole-body SPCCT clinical prototype to give an insight into its potential benefits for human imaging regarding image quality, diagnostic confidence, and a new approach to spectral CT imaging.

## SYSTEM CHARACTERISTICS

Compared with conventional CT with energy integrating, solid-state scintillation detectors, photon-counting CT uses direct converting detectors based on semiconductors, such as cadmium-telluride, cadmium-zinc-telluride, or silicon.<sup>1–5</sup> A high-bias voltage of 800 to 1000 V is applied between the semiconducting layer, so that impinging photons will be detected as electron-hole pairs, generating an electrical pulse, which is measured and registered by readout electronics into several energy bins according to the pulse height of the signal. Setting the lowest energy thresholds just above the electronic noise level allows complete elimination of noise from the signal chain. Therefore, the residual noise in the signal can be described as shot noise derived from the incoming photon statistics. The detector pixel size, typically ranging from 0.125 to 0.5 mm is defined by the size of the anode pads, which can be designed much smaller than in scintillating detectors as there is no need for optically non-transparent separation layers in semiconductors.<sup>4–6</sup> However, charge-sharing between neighboring pixels and the finite focal spot size of the x-ray tube sets a limit for the minimum reasonable pixel size, whereas pulse pile-up impacts the maximum detector pixel size.

The results presented in this review were acquired on a clinical SPCCT system prototype (Philips, Haifa, Israel), equipped with a 2-mm-thick cadmium-zinc-telluride, bonded to Philips' proprietary ChromAIX2 application-specific integrated circuit. The system enables a 500 mm in-plane field of view and a z-coverage of 17.6 mm in the isocenter, realized with 64 rows of detectors, 270 × 270 μm<sup>2</sup> in size. The application-specific integrated circuit supports the readout of 5 different energy bins with thresholds set at 30, 51, 62, 72, and 81 keV. The system specifications are summarized in Table 1. This system has been used in preclinical and clinical research studies to evaluate novel K-edge contrast materials and to investigate the potential of photon-counting CT in a clinical setting. However, the current system has some limitations, such as the small z-coverage and the lack of a complete set of clinical scan protocols, which need to be addressed for a full clinical implementation in the future to enable for example prospective electrocardiogram-gating, dose modulation, and faster scanning with a larger detector coverage.

Conventional CT images are obtained with this system by mapping the photon-counts in the 5 energy channels of each pixel to an equivalent water thickness before reconstructing the resulting sinogram data with a filtered back-projection algorithm.<sup>7</sup> For spectral image reconstruction, the photon-counting data are first decomposed into material-specific sinograms with a maximum-likelihood algorithm<sup>8,9</sup> and reconstructed afterward with an filtered back projection algorithm to obtain material base images, including additional denoising options such as a hybrid iterative reconstruction algorithm (iDose-like algorithm) for SPCCT (Fig. 1).

In the clinically relevant energy range of 30 to 140 keV, the photoelectric effect and Compton-scattering are the predominant physical

Received for publication November 8, 2022; and accepted for publication, after revision, January 20, 2023.

From the \*University Lyon, INSA-Lyon, University Claude Bernard Lyon 1, UJM-Saint Etienne, CNRS, Inserm, Villeurbanne, France; †Department of Radiology, Louis Pradel Hospital, Hospices Civils de Lyon, Bron, France; ‡Philips Healthcare, Suresnes, France; §Philips Healthcare, Haifa, Israel; and ||Philips Healthcare, Hamburg, Germany. Salim A. Si-Mohamed and Sara Boccacini are co-first authors with equal contribution.

Conflicts of interest and sources of funding: This work was supported by European Union Horizon 2020 grant no. 643694. Marjorie Villien, Yoad Yagil, and Klaus Erhard are employees of the manufacturer of the PCCT system.

Disclosures: Marjorie Villien, Yoad Yagil, Klaus Erhard are employees of the manufacturer of the PCCT system.

Correspondence to: Salim A. Si-Mohamed, MD, PhD, CHU Cardiologique Louis Pradel, Department of Cardiothoracic Radiology, 59 Boulevard Pinel, 69500 Bron, France. E-mail: salim.si-mohamed@chu-lyon.fr.

Copyright © 2023 The Author(s). Published by Wolters Kluwer Health, Inc. This is an open-access article distributed under the terms of the Creative Commons Attribution-Non Commercial-No Derivatives License 4.0 (CCBY-NC-ND), where it is permissible to download and share the work provided it is properly cited. The work cannot be changed in any way or used commercially without permission from the journal.

ISSN: 0020-9996/23/5807–0459

DOI: 10.1097/RLI.0000000000000965

**TABLE 1.** Main Characteristics of the Clinical Prototype

Parameter	SPCCT
Platform	Philips iCT
Supported scan modes	Axial, axial multicycles, helical
Tube voltages, kVp	80, 100, 120, 140
Tube currents, mA	10–500
X-ray filter	Half value layer HVL = 7.1 ± 0.7 mm at 120 kVp
Focal spot, mm × mm	0.6 × 0.7 × 2 (dual focal spots)
Gantry rotation, s	0.33, 0.4, 0.5, 0.75, 1.0
Projections per rotation	2400
Number of focal spots	2
Z-coverage in isocenter, mm	17.5
Number of detectors per row/column	64/1848
Field of view, mm	500
Pixel pitch, μm × μm]	274 × 274 μm <sup>2</sup> at isocenter
Electronic readout	Philips ChromAIX2
Number of energy thresholds	5
Sensor material	Cadmium Zinc Telluride, 2 mm thickness

SPCCT indicates spectral photon-counting computed tomography.

effects characterizing the interaction of x-rays with biological tissue. Hence, the spectral attenuation of human tissue can be well approximated in the projection domain by a linear combination from these 2 energy-dependent effects, as well as some spatially varying, but energy-independent, weights.<sup>10</sup> With a fully polychromatic forward model, beam-hardening effects can be included and therefore, theoretically, eliminated from the spectral image reconstruction.<sup>11,12</sup>

**CLINICAL APPLICATIONS**

**General Benefits of SPCCT Imaging**

Spectral photon-counting CT technology is known to have several benefits over current CT systems that are equipped with energy-integrating detectors (EID-CT). It increases spatial resolution by a factor of ~4,

with an achievable voxel size of 0.15 to 0.25 mm<sup>3</sup> for all applications, including lung, ear, musculoskeletal, coronary artery, and vessel imaging. It decreases the radiation dose by 30% to 50% while providing a similar noise level to that of EID-CT images by suppressing electronic noise.<sup>4,13–18</sup> It enhances tissue contrast for a similar energy beam to that of EID-CT images owing to the constant weighting of photons, leading to greater weighting of the low-energy photons carrying the photoelectric effect, whereas EID-CT technology uses linear weighting. Moreover, SPCCT decreases beam-hardening-like artifacts and blooming artifacts owing to higher spatial resolution, despite an increase in CT attenuation of all high-contrast tasks. It enables better energy sampling of the transmitted spectrum than dual-energy CT technology, that is, more than 2 energies. This leads to greater discrimination between low- and high-energy photons than with EID-dual-energy computed tomography technology and therefore to higher resolution of photoelectric and Compton effects. As a result, SPCCT may improve the performances of any type of virtual images such as virtual monochromatic, virtual noncontrast, Z-effective, electronic density, as well as any type of material decomposition process like that of water or iodine imaging.<sup>19,20</sup> Altogether, these advantages hold great promise for changing the current workflow of CT (Fig. 2). More importantly, radiologists should understand that SPCCT offers all these advantages in just 1 scan, as shown in our experiments (Tables 2 and 3), without increasing the dose, changing the technical parameters, or requiring spectral mode prospectively. This key feature should provide great leverage to help spread the use of SPCCT technology.

**Conventional Imaging**

**Lung Applications**

Computed tomography is the mainstay of lung imaging owing to its higher spatial resolution, convenience, availability, and faster acquisition time than with other imaging methods such as magnetic resonance imaging or nuclear imaging. However, CT often requires additional histological analyses or other types of nonradiological examinations for accurate diagnosis and would therefore benefit from better detection and characterization of parenchymal lesions while reducing x-ray dose. Accordingly, in the following subsections of this review, we present some key applications that, based on our experience, could benefit from ultra-high-resolution (UHR) performances. These could be achieved with radiation doses that are similar to/lower than current CT systems

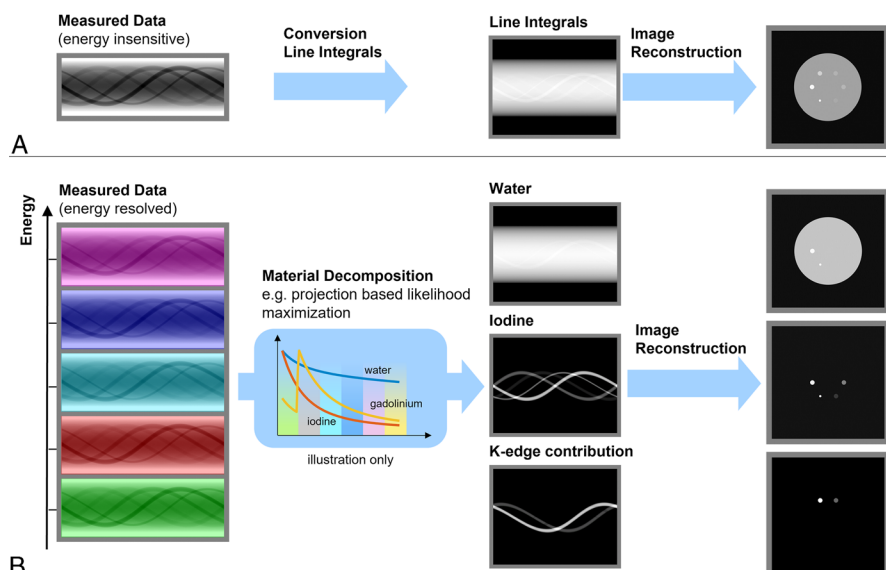


**FIGURE 1.** Diagram to illustrate the 2-stage process used for generating SPCCT images through an energy insensitive process for conventional imaging (A) and an energy resolved material decomposition process for spectral images (photoelectric, Compton, K-edge(s)) (B).

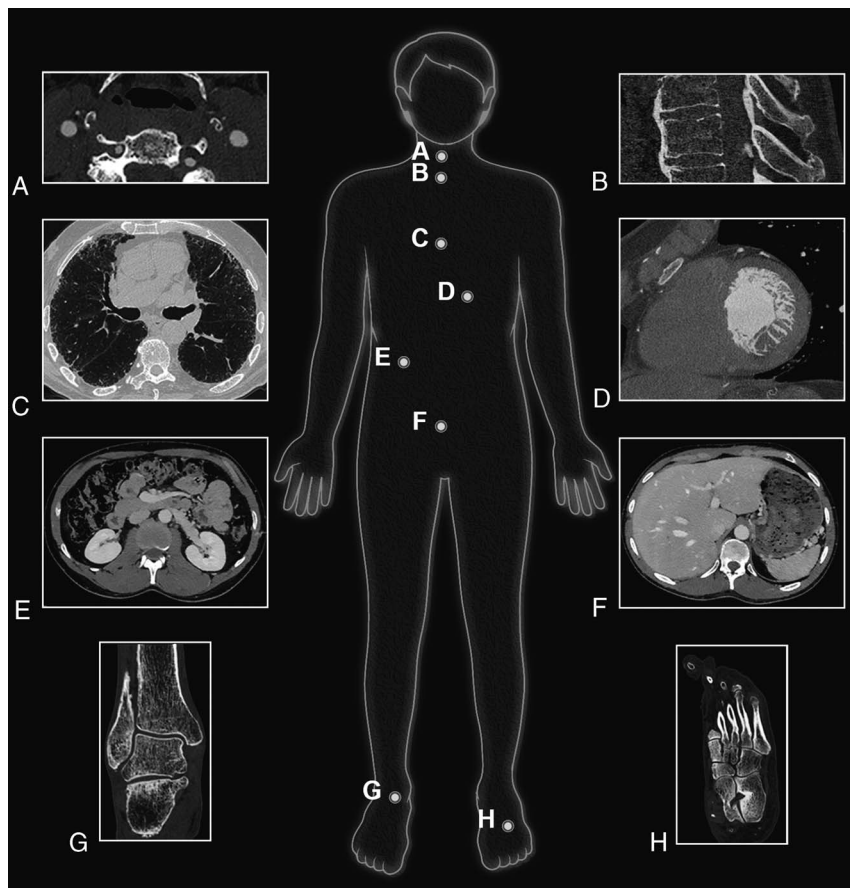


**FIGURE 2.** Illustration of clinical experience with numerous clinical applications using a whole-body clinical SPCCT prototype (Philips Healthcare) on a research platform at the University of Lyon.

by taking advantage of the higher matrix size (eg, 1024–2048), thinner slice thickness (eg, down to ~0.15 mm), and higher frequency filters.<sup>13,18,28,29</sup>

**Lung Nodule Imaging**

Spectral photon-counting CT detects lung nodules very well. In a phantom study in which we performed a task-based image quality

assessment of nodule imaging,<sup>23</sup> we found that noise magnitude was reduced whereas the spatial resolution improved, leading to greater detectability of solid and ground-glass nodules (GGNs) than with EID-CT. Interestingly, the detectability gap between the different platforms was more pronounced for the GGNs, which can be explained by SPCCT's higher gain in detectability of low-contrast tasks. For example, we found

**TABLE 2.** Overview of the Clinical SPCCT Protocols and Their Specificity

Organ	Applications	Specific Mode	Voxel Size	Radiation Dose Protocols
Cardiac imaging	Coronary CT angiography	Helical/retrospective ECG-gating scans	0.21 × 0.21 × 0.25 mm	Low and standard dose
	Valve imaging	Helical/retrospective ECG-gating scans	0.21 × 0.21 × 0.25 mm	Low and standard dose
	Late phase cardiac CT	Helical/retrospective ECG-gating scans	0.21 × 0.21 × 0.25 mm	Low and standard dose
Lung imaging	ILD screening	Noncontrast helical CT scans	0.29 × 0.29 × 0.25 mm	Low dose
	Lung nodule screening	Noncontrast helical CT scans	0.29 × 0.29 × 0.25 mm	Ultra and low dose
	COVID	Noncontrast helical CT scans	0.29 × 0.29 × 0.25 mm	Low dose
	CTEPH	Noncontrast helical CT scans	0.29 × 0.29 × 0.25 mm	Standard dose
Musculoskeletal imaging	Foot	Noncontrast helical CT scans	0.15 × 0.15 × 0.25 mm	Low and standard dose
	Knee	Noncontrast helical CT scans	0.15 × 0.15 × 0.25 mm	Low and standard dose
Vascular imaging	Carotid vascular and plaque imaging	Contrast helical scans	0.21 × 0.21 × 0.25 mm	Low and standard dose
	Aortic imaging	Contrast helical scans	0.21 × 0.21 × 0.25 mm	Low and standard dose
Abdominal imaging	Adrenal gland	Contrast helical scans	0.21 × 0.21 × 0.25 mm	Low and standard dose

SPCCT indicates spectral photon-counting computed tomography; CT, computed tomography; ECG, electrocardiogram; ILD, interstitial lung disease; CTEPH, chronic thromboembolic pulmonary hypertension.

**TABLE 3.** Summary of Additional Benefits Using the Clinical SPCCT Prototype (Philips Healthcare) Compared With EID-CT in Human Clinical Research

Images	Organ	Application	Additional Outcomes	Reference
Ultra-high-resolution images	Heart	Coronary artery lumen	Improvement of diagnostic quality by a factor of 2	14
			Improvement of diagnostic confidence for half of the cases	14
		Coronary artery stent	Improvement of stent lumen and structure visualization	14,21 Figure 7
			Reduction of blooming artifacts and intraluminal artifacts	14,21 Figure 7
		Coronary artery plaque	Improvement of diagnostic quality by a factor of 2	14
			Improvement of diagnostic confidence for half of the cases	14
		Calcium scoring	More accurate quantification of the calcium volume	22
	Lung	Distal airways	Clearer visualization up to 5th level	13 Figure 6
		Distal vessels	Improvement of their sharpness and conspicuity	13
		Nodule	Improvement of detectability by a factor of 2	13,23
		Improvement of accuracy quantification	24	
		Improvement of characterization	13,24	
Low- and ultra-low-dose images	Chest	Nodule imaging	Improvement of the nodule sharpness and conspicuity	13
	Heart	Calcium scoring	Higher accuracy for low dose condition	25
Virtual monochromatic images	Heart	Coronary artery lumen	Improvement of diagnostic quality of distal lumen	14,26
	Aorta	Vascular imaging	Improvement of lumen opacification	14
	Pulmonary arteries	Vascular lung disease	Improvement of lumen opacification	Figure 11
	Carotid vessels	Carotid lumen	Improvement of lumen opacification	27
Iodine images	Carotid vessels	Carotid lumen	Specific visualization of the lumen	27
	Chest	Lung perfusion	Specific visualization of the lung microangiography	Figure 12
	Heart	Myocardial perfusion	Specific visualization of the myocardial perfusion	Figure 12

SPCCT indicates spectral photon-counting computed tomography; EID-CT, computed tomography equipped with energy-integrating detectors.

that, under low-dose conditions, a 2 mm GGN barely noticeable with EID-CT could be visualized with SPCCT. In addition, we found that stronger levels of iterative reconstruction could be used with SPCCT than with EID-CT. This is because of a lower loss in spatial resolution and impact on noise texture than iterative reconstruction with EID-CT, leading to a more drastic dose optimization and radiologists' acceptance of the technology.

Spectral photon-counting CT quantifies lung nodule volumes more accurately. In a phantom study, we found that, compared with the high-resolution mode of EID-CT, SPCCT estimated the volume of solid round nodules—with or without spikes—much better, despite an underestimation compared with the ground-truth,<sup>24</sup> as previously reported.<sup>30</sup> Nevertheless, it still provided more precise, robust markers of the evolution of lung nodules.

Spectral photon-counting CT can characterize lung nodule shapes and components more accurately. In a phantom study, we found that SPCCT estimated the shape of solid nodules more accurately than high-resolution EID-CT, leading to more precise identification of the surrounding tissues. This would be particularly helpful for characterizing their relationship with the vessels suggested as a marker of malignancy.<sup>31,32</sup>

To conclude, a GGN case study is provided in Figure 3 to illustrate all these expectations.

### Diagnosis of Pulmonary Fibrosis and Its Confidence

Fibrotic key features can be more easily visualized with SPCCT, leading to better diagnostic confidence for pulmonary fibrosis. In our experience, SPCCT improved the detection of all fibrotic lesions and, more specifically, early fibrotic lesions, such as intralobular reticulation and bronchiolectasis, that are barely visible on EID-CT. This could lead to earlier diagnosis and would play an important role in managing patients

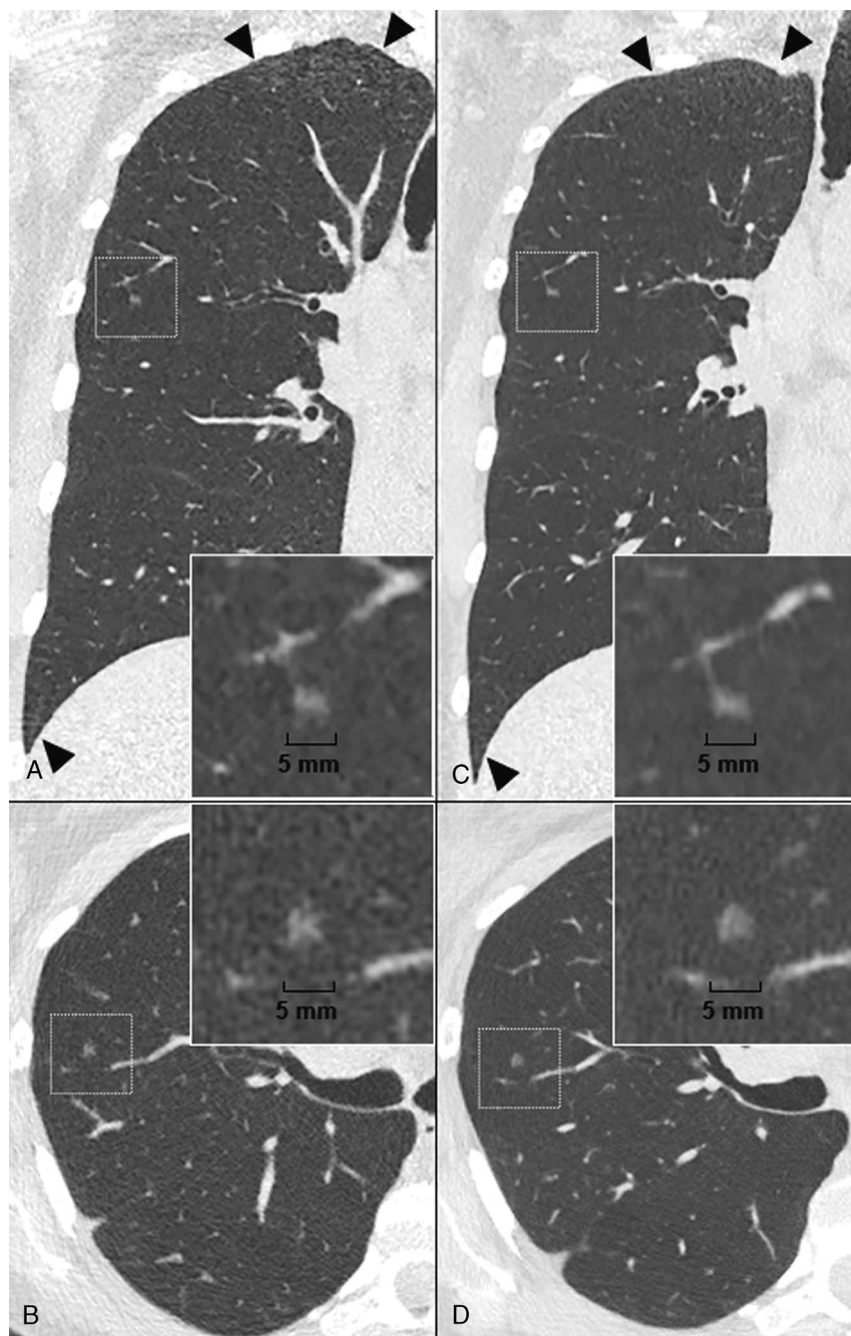
with a high risk of developing pulmonary fibrosis associated with systemic sclerosis, pneumoconiosis, chronic tobacco use, or long-term residual COVID-19 (Fig. 4). This result corroborates the outcome of the study by Inoue et al,<sup>33</sup> who showed that SPCCT outperformed EID-CT in terms of image quality for diagnosing reticulation, ground glass opacities, and mosaic patterns while giving a higher probability score for usual interstitial pneumonia (UIP). In addition, SPCCT improves the delineation of all fibrotic lesions, making it easier to differentiate between bronchiolectasis and honeycombing. Our initial study with lung UHR SPCCT imaging found that subpleural cystic lesions (which would otherwise have been identified as honeycombing) were connected to the peripheral bronchiectasis. Consequently, a significant number of cases of "typical UIP" may actually be "probable UIP" according to the Fleischner Society's definition.<sup>34</sup> In the near future, this should be considered for interstitial lung disease classification (Fig. 5). Altogether, these key features in particular would help to characterize and quantify fibrosis biomarkers (known as markers of severity) more precisely, using manual or automatic deep learning–based segmentation.<sup>35</sup>

### Imaging for Acute or Chronic Pulmonary Embolism

Spectral photon-counting CT allows greater detection of acute and chronic pulmonary embolism. In our study, the vascular features related to pulmonary embolism were more easily identifiable in arteries up to the subsegmental territories (Fig. 5). This was the case for small bands and webs barely visible on EID-CT, leading to a significant increase in the clot burden. This would be particularly helpful to guide the current therapeutic strategy, either for surgical or endovascular treatment.

### Imaging for Small Airway Diseases

Small airway diseases can be more easily evaluated with SPCCT. In the study of a healthy human volunteer, we demonstrated improved



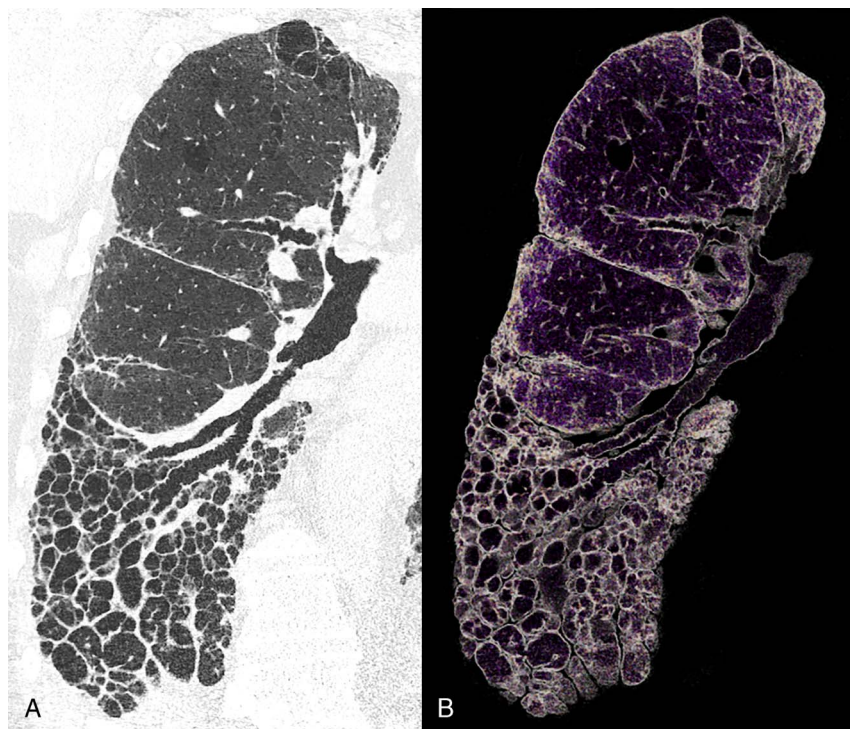
**FIGURE 3.** Case study of a pure ground glass nodule (GGN) on a lung low-dose ultra-high resolution (LD-UHR) imaging in a 44-year-old woman using energy-integrating dual-layer detector CT (EID-DLCT; CT7500) and SPCCT systems (Philips Healthcare) (A–B, coronal and axial EID-DLCT images; C–D, coronal and axial SPCCT images; in small boxes, zoom magnification of the GGN). Compared with EID-DLCT, SPCCT images lead to a better, comprehensive assessment of GGN, showing a round shape, a higher volume confirmed by an automatic segmentation ( $30.6 \text{ mm}^3$  vs  $24 \text{ mm}^3$ , ie, an 25% increase) and a link with a fine vessel from an adjacent segmental pulmonary vein/artery, possibly suggestive of adenomatous hyperplasia. SPCCT images also show the reduction in noise in the upper and lower part of the lungs (black arrowheads).

image sharpness and conspicuity of the distal airways and their walls up to fourth-order bronchi.<sup>13</sup> In patients, SPCCT gave excellent visualization of the bronchial walls for monitoring their thickening as well as centrilobular micronodules like those seen in obliterative bronchiolitis (Fig. 6).<sup>36</sup> In addition, SPCCT increases the contrast of air-trapping, leading to better visualization of mosaic patterns as previously demonstrated.<sup>33,36</sup> This feature would be particularly helpful for monitoring

the response to treatment and predicting the exacerbations of respiratory diseases like chronic obstructive pulmonary disease more accurately.<sup>37</sup>

### Cardiac Applications

For years, coronary CT has been regarded as the gatekeeper to further investigations, especially invasive coronary angiography, and is now recommended as the first-line examination of choice for



**FIGURE 4.** Case study of a combined pulmonary fibrosis and emphysema on lung low-dose UHR imaging (LD-UHR) in a 73-year-old man using an SPCCT system (Philips Healthcare) (A, coronal oblique with  $0.29 \times 0.29 \times 0.25$  mm voxel size; B, 3-mm-width volume rendered image). With SPCCT images, fibrotic lesions can be fully assessed up to the periphery, allowing depiction of intralobular and interlobular reticulation, subpleural cysts, and differentiation between bronchiolectasis and honeycombing. The radiological pattern was considered as probable UIP on SPCCT, whereas it was noted as atypical UIP on the EID-CT image.

investigating coronary pathologies.<sup>38</sup> The remaining limitations of coronary CT include assessment of the lumen when there is heavily calcified plaque or stents, especially small ones, and the analysis of plaque components. Furthermore, first-pass perfusion CT can complete coronary CT examinations by providing information on the hemodynamic significance of coronary stenosis.<sup>39</sup> Late-enhancement areas can be detected by late phase acquisition indicating, among other things, myocardial infarction or myocarditis.<sup>40</sup> Nevertheless, analyzing the myocardium can be difficult because of the low contrast resolution of EID-CT. Computed tomography angiography also has a central place in preinterventional and presurgical planning for valve pathologies.<sup>41,42</sup> However, this type of scan is mainly used for measuring, not for primary diagnosis, as the valves are difficult to assess because of their very thin structure. Spectral photon-counting CT can potentially overcome most of these limitations.

#### Coronary Lumen Assessment

Blooming artifacts can be reduced with SPCCT by improving spatial resolution. Calcification and stent analysis can prove cumbersome with EID-CT mainly because of blooming artifacts but can probably be improved with SPCCT. Indeed, phantom experiments have shown that the volume of calcifications is smaller, and closer to the reality, with SPCCT than with EID-CT.<sup>43</sup> In humans, the reduction of blooming artifacts leads to a better estimation of lumen permeability.<sup>14</sup> The same applies to coronary stents both in phantoms<sup>44</sup> and in humans.<sup>21</sup> Blooming artifacts are reduced, resulting in a thinner appearance of the stent structure. Thereafter, it is easier to assess the lumen and intrastent lesions, as well as of the surrounding structures, including calcifications, as previously published<sup>14,21,44,45</sup> and shown in Figure 7. Subjective image quality is also much better than with EID-CT.<sup>21</sup> This

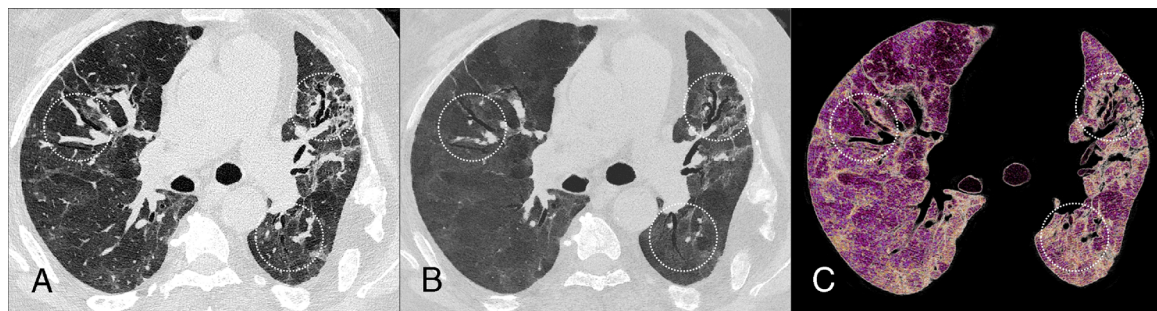


**FIGURE 5.** Case study showing post-COVID-19 pulmonary fibrosis with lung low-dose UHR imaging (LD-UHR) in a 69-year-old man using an SPCCT system (Philips Healthcare) (A, axial image; B, 3-mm-width minimal-intensity projection image; C, 3-mm-width volume rendering image). Pulmonary functional tests showed a restrictive disorder with forced vital capacity and a forced expiratory volume in 1 second at 36% and 43% of the theory, respectively. SPCCT images facilitated the identification and characterization of multiple varicoid traction bronchiectasis and reticulation within foci of fibrosis (dotted circles). Note that mosaicism can be seen on both native and minIP images, probably due to air trapping.

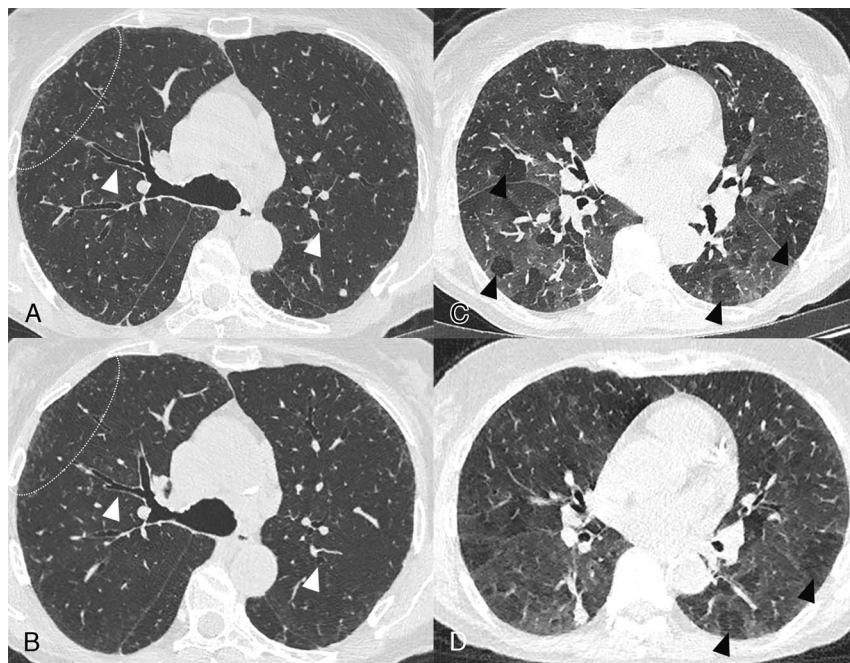


**FIGURE 6.** Case study of obliterative bronchiolitis associated with rheumatoid arthritis on lung UHR (LD-UHR) imaging in a 68-year-old woman using an SPCCT system (Philips Healthcare) (A and C,  $0.29 \times 0.29 \times 0.25$  mm voxel size axial images) and an EID-CT (B and D,  $0.58 \times 0.58 \times 0.67$  mm voxel size axial images) (A–B, inspiratory images; C–D, expiratory images: axial image). SPCCT images allow better visualization of the bronchial wall (white arrowheads), the peripheral centrilobular micronodules (dotted white circle), and mosaicism on expiratory images due to air trapping.

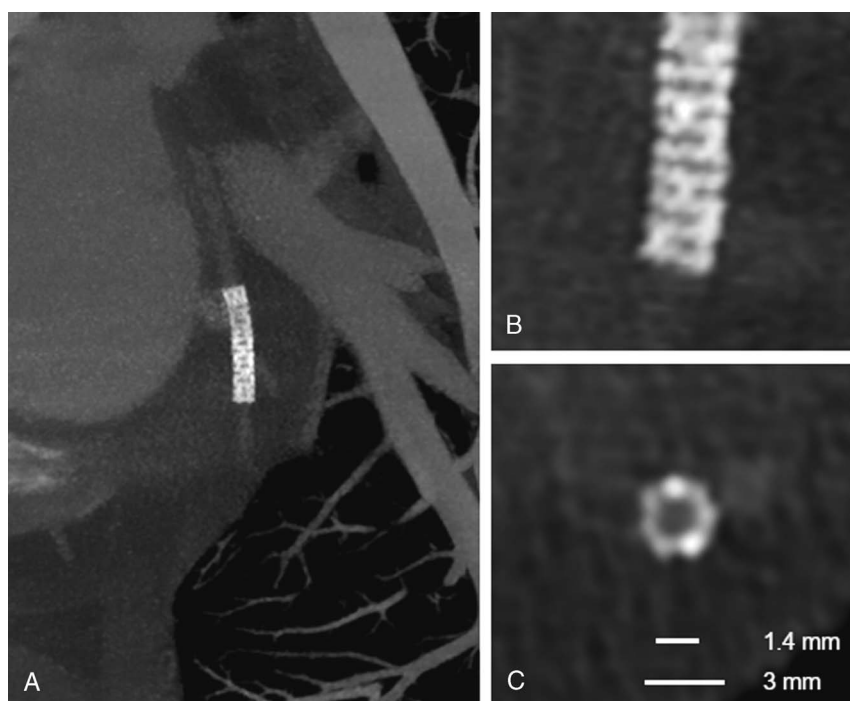


**FIGURE 7.** Multiplanar maximal-intensity projection reconstructions with different thicknesses highlight the structure of this small stent of the circumflex artery obtained with a coronary angiography using a SPCCT system (Philips Healthcare). In A, the entire stent is shown. In B, a detail of the distal extremity of the stent nicely demonstrates the structure of the stent struts despite the small dimensions. This is possible thanks to reconstruction with a high matrix ( $1024 \times 1024$ ), thin slice thickness (0.25 mm), and sharp kernel. In C, a cross-sectional plane of the stent clearly demonstrates its structure and the patent lumen. Notice that the internal stent diameter was of 1.4 mm and the external diameter was 3 mm.

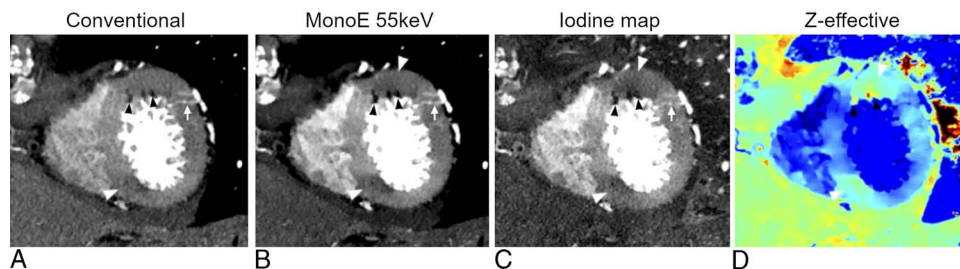


**FIGURE 8.** An example of multiparametric imaging (A, conventional image; B, MonoE 55 keV; C, iodine map; D, Z-effective) of myocardial perfusion anomalies of the left ventricle as assessed on a short axis apical plane of a cardiac angiography using an SPCCT system (Philips Healthcare). Conventional images (A) showed a few small hypodense spots (black arrowheads) of the anterior segment, possibly adipose metaplasia. These lesions were also visible on spectral images (arrowheads in B, C, D) and also showed an adjacent area of hypoperfusion (white arrows) with transmural extension but more pronounced in the subendocardial layer. The combination of adipose remodeling and hypoperfusion raised the suspicion of myocardial infarction. A second area of hypoperfusion of the inferior wall, also more obvious in the subendocardial layer, could be spotted with some difficulties on conventional images (arrowhead in A) but very easily on the spectral images (arrowhead in B, C, D). In addition, the perforating branches of the diagonal coronary artery (arrow in A, B, C) providing supplementary vascularization to the infarcted area can be easily seen.

improved performance should result in a reduction of invasive coronary angiography for patients with heavily calcified coronary arteries and small stents.

#### Plaque Characterization and Calcification Assessment

Plaque components are more easily characterized with SPCCT and calcification is detected and assessed more specifically. Although certain features of vulnerable plaque can be identified with EID-CT, it is still unfeasible for distinguishing soft tissue components. With SPCCT, because of the increase in spatial resolution, the relative volume of different components can be better estimated.<sup>46</sup> In an ex vivo sample, intraplaque fat can be distinguished from the vascular wall as well as from perivascular adipose tissue owing to differences in photoelectric and Compton effects, which needs to be investigated in vivo.<sup>47</sup> All these features combined together are expected to greatly improve plaque characterization and facilitate the detection of plaque prone to rupture. Nevertheless, the current knowledge might need to be updated as more and more accurate information on plaque composition becomes available. Another classification that will most likely necessitate adjustments is calcium score. First, phantom SPCCT studies<sup>22,25</sup> show that a higher number of smaller-sized calcifications can be detected, which, if confirmed in human, might result in reclassification and risk stratification. In addition, although the calcium score calculated with well-established parameters is comparable between EID-CT and SPCCT, contrast-to-noise ratio is higher with SPCCT<sup>48</sup> and the density of calcifications is different depending on both CT system and slice

thickness.<sup>22</sup> Thanks to improved cardiovascular risk prediction and stratification with SPCCT, patients will likely benefit from more tailored prevention and therapy, the effect of which would be identified with SPCCT follow-up.

#### Myocardial Assessment

Spectral photon-counting CT allows better contrast resolution of soft tissues, including the myocardium. In our experience, differences in myocardial first-pass perfusion at rest are easier to detect with SPCCT (Fig. 8) than with EID-CT. Late enhancement areas are also easier to locate within the myocardium even at a high kilovoltage peak (eg, 120 kVp). These properties can be further improved by spectral imaging (see Subsection Virtual Monochromatic Imaging and Material Decomposition Into 2 Materials). Therefore, the extracellular volume calculation is expected to be more precise, even with just 1 acquisition. We expect these features to result in a broader use of perfusion-CT with better diagnostic confidence designating SPCCT as a one-stop-shop for coronary artery disease, a role once anticipated for EID-CT, but never completely fulfilled. In addition, SPCCT will play a central role in diagnosing acute myocardial disease alongside, or instead of, cardiac magnetic resonance imaging.

#### Other Cardiac Structures

Very small structures can be visualized with SPCCT, and valve leaflets like those in Figure 9, chordae, trabeculae, and other small cardiac structures all benefit from SPCCT's improved spatial resolution.<sup>14</sup> The expected clinical benefits are numerous, ranging from improved

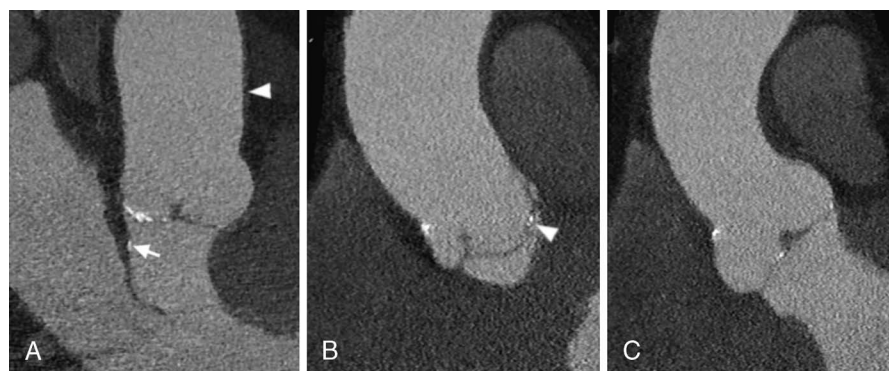


**FIGURE 9.** Three multiplanar reconstructions (A–C) of a cardiac angiography using an SPCCT system (Philips Healthcare) showing small calcifications of the 3 leaflets of the aortic valve. In A, also a very thin calcification of the left ventricular outflow tract (arrow) adjacent to the anterior mitral leaflet is well depicted. In the same panel, the wall of the aorta can be seen (arrowhead), although it is of normal thickness without obvious atherosclerosis. In B, notice how the position of the calcification regarding the 3 layers of the aortic valve leaflets (arrowhead) can be well appreciated.

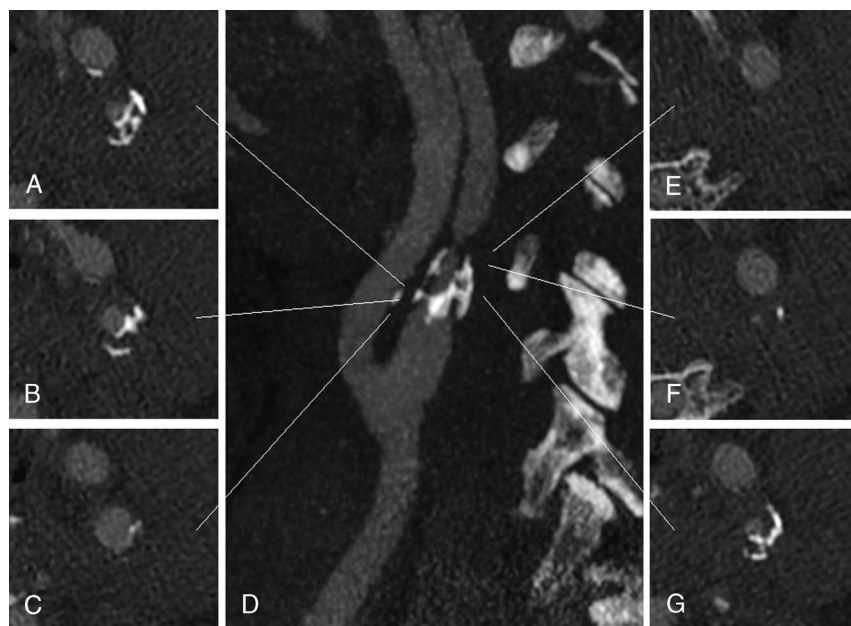


**FIGURE 10.** UHR carotid angiography using an SPCCT system (Philips Healthcare) showing severe stenosis of the left internal carotid artery due to mixed atheromatous plaque visible on the axial planes (A–C and E–G) at different levels of the artery (white lines) as shown on a maximal-intensity projection parasagittal image (D). Thanks to the improved spatial resolution of SPCCT subsequent reduction of artifacts, these images, reconstructed with a matrix of 1024 and a thickness of 0.25 mm, allow depiction of the complex structure of the calcifications as well as the soft tissue components of the plaque. In addition, the lumen of the vessel is clearly assessable, even when punctiform (F and E).

valvular analysis to easier diagnosis of cardiomyopathies such as noncompaction.

### Vascular Imaging

As very thin vessels can be visualized with SPCCT, the degree of stenosis in heavily calcified vessels can be better estimated (Fig. 10) and intrastent pathologies are more easily visualized. Structures that will particularly benefit from these features include carotid arteries<sup>27,49</sup> and vertebral arteries for which, in addition to the aforementioned general limitations of EID-CT, the proximity to bones can prove particularly detrimental for correct lumen assessment. Blooming and other artifacts are reduced by SPCCT, allowing the precise assessment of very severe vertebral artery stenosis caused by osteophytes.<sup>27</sup> Furthermore, as in our experience, the interface between patent lumen and plaque is

better delineated with SPCCT; small ulcers and irregularities of plaques and intimal layers should also be easier to detect. As the smaller, more distal, more calcified vessels and the arteries adjacent to bones and with stents will be assessable, diagnostic invasive angiography procedures are expected to become anecdotal.

### Miscellaneous

Spectral photon-counting CT has shown benefits for applications in various anatomical areas. Bone structure is better delineated, with particularly impressive improvements for trabecular bone (Fig. 11), facilitating the detection of anomalies such as metastasis<sup>50</sup> and myeloma lesions.<sup>51</sup> Cartilage in the knee and subchondral lesions, as well as soft tissues such as tendons, can also be easily visualized with SPCCT<sup>52</sup> (Fig. 11). Finally, the temporal bone and the small bones

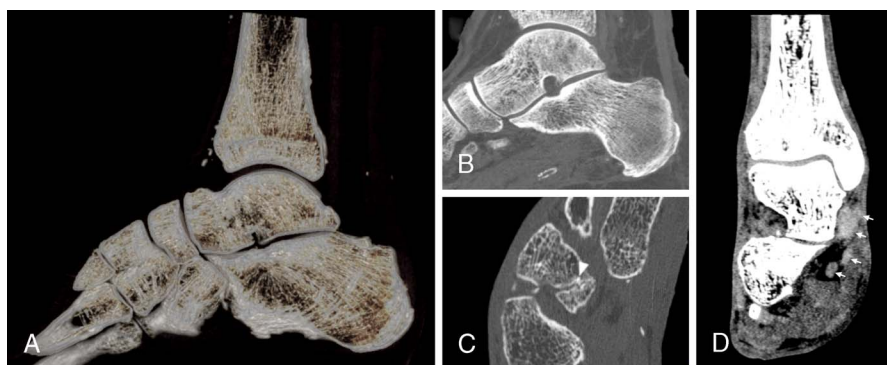


**FIGURE 11.** Noncontrast acquisition using an SPCCT system (Philips Healthcare) of the foot of a 38-year-old patient with diabetes and gait troubles. A, Volume rendering of the bones of the ankle showing the details of the trabeculae thanks to reconstruction with a 1024 matrix and sharp kernel. These are visible also on the maximal-intensity projection detail of the talus and calcaneus in B. C, Detail of the cuboid-navicular joint with reduction of the articular space and a small calcification (arrowhead) between the 2 cortexes determining a subchondral lesion of the navicular bone. Not only bone structures are better visible with SPCCT as compared with EID-CT: in D, with a softer kernel, tendons of the lateral compartment of the ankle (arrows) are clearly distinguishable from each other and from other tissues. This seems to be true for both pathologically thickened tendons (such as the tibialis posterior) and normal ones.



**FIGURE 12.** Case study of VMI for an UHR pulmonary angiography using an SPCCT system (Philips Healthcare) in a 39-year-old woman with chronic thromboembolic pulmonary hypertension (A–B, 40-mm width maximal-intensity projection coronal 70 keV [A] and 40 keV [B], 40-mm width volume rendering coronal 70 keV [C] and 40 keV [D]). Virtual monochromatic images and more particularly at 40 keV show numerous vascular features on central and peripheral arteries of chronic pulmonary embolism including endoluminal band (white arrowheads), stenosis and poststenosis dilatation of pulmonary arteries (white arrows), vessel pruning, and poor distal perfusion (white dotted circles).

of the internal ear can be better depicted with SPCCT than with EID-CT, and certain structures receive subjective scores, indicating almost perfect image quality.<sup>53</sup> In all, although CT is already the imaging modality of choice for assessing bone morphology, it could be further improved by SPCCT and even used to enhance detection of diseases like osteitis and secondary lesions in the early stages.

For abdominal applications, a combination of all the previously mentioned features of SPCCT would help improve the image quality of different organs and diseases. Nevertheless, because most abdominal

pathologies affecting organs like the liver, spleen, kidneys, and pancreas are visible, owing to differences in contrast between normal parenchyma and lesions, most advantages are expected to be derived from the spectral properties of SPCCT.

### Low- and Ultra-Low-Dose Imaging

With SPCCT, the x-ray dose is significantly reduced compared with EID-CT. In our experience, the overall dose decreased by 5%, with reductions of ~40% and ~10% for cardiac and lung applications,

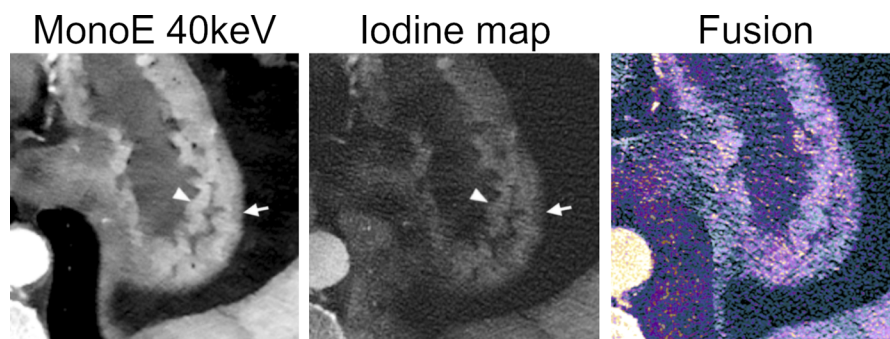


**FIGURE 13.** An example of multiparametric imaging of the gastric wall on an abdominal angiography using an SPCCT system (Philips Healthcare). Monoenergetic images at low energy and the iodine map nicely show the different perfusion of the rugae of the mucosa (arrowheads) and the submucosal layer (arrows). The dataset fusing conventional images (gray) and iodine images (color coded) can help visual assessment of any eventual hypoperfused area.

respectively. Altogether, the benefits of SPCCT are expected to offer a more efficient tool for low- and ultra-low-dose strategies for lung-screening, pediatric imaging and iterative follow-up of cancer or chronic disease management.<sup>54</sup>

### Virtual Monochromatic Imaging

Virtual monochromatic imaging (VMI) is a tool already available on all dual-energy CT platforms. At low-energy, that is, 40 keV, VMI enables an increase in CT attenuation of iodine and more generally of tissue with high photoelectric absorption. This improves contrast-to-noise ratios of enhanced lesions or vessels<sup>55,56</sup> and decreases the iodine load for a satisfactory level of vessel opacification.<sup>57–59</sup> At higher energy than 70 keV, VMI enables a reduction of beam-hardening like-artifacts, thus improving the visualization of tissues surrounding high-attenuating tissues, iodinated vessels,<sup>60</sup> or metallic structures such as stents or prostheses.<sup>61,62</sup> In our experience, the advantages of using VMI with SPCCT rely in the combination of all the technical benefits, that is, an improved spatial resolution, an improved discrimination between photoelectric and Compton effects, as well as a greater dose efficiency and weighting of the low-energy photons. Altogether, VMI coupled with SPCCT should allow, for example, UHR pulmonary SPCCT angiography for a better evaluation of chronic thromboembolic pulmonary hypertension (Fig. 12) and UHR coronary SPCCT angiography to identify the distal coronary arteries<sup>14,26</sup> and better visualize myocardial ischemia/infarction (Fig. 8).

### Material Decomposition Into 2 Materials

Material decomposition imaging into 2 materials is already available on dual-energy CT platforms but appears to be much improved because of all the previously listed advantages. Material decomposition allows each tissue to be projected into 2 materials of different known linear absorption coefficients. Therefore, it cannot specifically discriminate tissues with linear absorption coefficients at a similar distance from the chosen materials, such as calcium, which is distributed into water and iodine images. Nevertheless, these maps have many advantages, including functional evaluation of organ perfusion such as in the myocardium,<sup>55</sup> lung,<sup>63</sup> or digestive tract (Fig. 13).

### Color K-Edge Imaging

The advantages mentioned above, although illustrating some basic but important advantages of SPCCT over conventional CT imaging, still do not emphasize the most groundbreaking contribution of SPCCT: color K-edge imaging. Color K-edge imaging places the energy bin boundaries in close proximity to the K-edge energies of elements, defined as the binding energy between the inner electronic layer and the atom. This means that the contrast agent can be identified specifically and quantitatively, allowing concomitant specific imaging of K-edge contrast agents like gold and gadolinium and their differentiation from surrounding tissue and non-K-edge contrast agents such as iodine-based agents.<sup>1,5,64–82</sup> This new approach may be an advantage for exploring new approaches such as for performing a biphasic organ CT imaging by providing simultaneously a specific enhancement after a consecutive injection of iodine- and gadolinium-based contrast agents<sup>71</sup> or for performing a molecular CT imaging by monitoring the macrophage burden within the high-risk atherosclerotic plaques.<sup>70</sup> Despite the multiple preclinical studies taking advantage of color K-edge imaging, translation in humans still has to be developed.

### CONCLUSION

The introduction of spectral photon-counting CT in the clinical field has opened a new chapter for medical imaging. The expectations in terms of improved image quality are already being demonstrated for many applications, including those most in need of better spatial resolution and contrast, as well as reduced radiation dose. Altogether,

SPCCT is expected to provide significant benefits for disease diagnosis, characterization, and staging and to open to new approaches that were not previously available in the field of CT. However, SPCCT systems are still scarce and the use of this technology needs to spread.

### ACKNOWLEDGMENT

We acknowledge Hugo Lacombe, Angele Houmeau, Bernard Martin, Pierre Lin-Wee-Kuan, Mouhammad Varasteh, Pierre-Antoine Rodesch, Bernhard Brendel, Philippe Coulon, Vincent Cottin, Myriam Moret, Daniel Bar-ness, Julie Traclet, Mouhammad Nasser, Kais Ahmad, François Lestelle, Valérie Leitman, Cyril Prieur, Jerome Prat, Arthur Pelat, Adeline Mansuy, Morgane Bouin, Apolline Barbe, Jean-Baptiste Langlois, Franck Lavenne, and CERMEP Facility and their employees for their help in conducting this clinical research experience. We thank Teresa Sawyers Teresa Sawyers, medical writer at the BESPIM, Nîmes University Hospital, for her help in editing the manuscript.

### REFERENCES

- Si-Mohamed S, Bar-Ness D, Sigovan M, et al. Review of an initial experience with an experimental spectral photon-counting computed tomography system. *Nucl Instrum Methods Phys Res Sect Accel Spectrometers Detect Assoc Equip.* 2017;873:27–35.
- Rajendran K, Petersilka M, Henning A, et al. First clinical photon-counting detector CT system: technical evaluation. *Radiology.* 2022;303:130–138.
- da Silva J, Grönberg F, Cederström B, et al. Resolution characterization of a silicon-based, photon-counting computed tomography prototype capable of patient scanning. *J Med Imaging (Bellingham).* 2019;6:043502.
- Taguchi K, Iwanczyk JS. Vision 20/20: single photon counting x-ray detectors in medical imaging. *Med Phys.* 2013;40:100901.
- Greffier J, Villani N, Defez D, et al. Spectral CT imaging: technical principles of dual-energy CT and multi-energy photon-counting CT [published online ahead of print November 19, 2022]. *Diagn Interv Imaging.* S2211-5684(22)00221-2.
- Ballabruga R, Alozy J, Bandi FN, et al. Photon counting detectors for x-ray imaging with emphasis on CT. *IEEE Trans Radiat Plasma Med Sci.* 2021;5:422–440.
- Heuscher D, Brown K, Noo F. Redundant data and exact helical cone-beam reconstruction. *Phys Med Biol.* 2004;49:2219–2238.
- Roessl E, Brendel B, Engel K-J, et al. Sensitivity of photon-counting based K-edge imaging in x-ray computed tomography. *IEEE Trans Med Imaging.* 2011;30:1678–1690.
- Schlomka JP, Roessl E, Dorscheid R, et al. Experimental feasibility of multi-energy photon-counting K-edge imaging in pre-clinical computed tomography. *Phys Med Biol.* 2008;53:4031–4047.
- Alvarez RE, Macovski A. Energy-selective reconstructions in x-ray computerized tomography. *Phys Med Biol.* 1976;21:733–744.
- Alvarez RE. Near optimal energy selective x-ray imaging system performance with simple detectors. *Med Phys.* 2010;37:822–841.
- Roessl E, Proksa R. K-edge imaging in x-ray computed tomography using multi-bin photon counting detectors. *Phys Med Biol.* 2007;52:4679–4696.
- Si-Mohamed S, Boccalini S, Rodesch P-A, et al. Feasibility of lung imaging with a large field-of-view spectral photon-counting CT system. *Diagn Interv Imaging.* 2021;102:305–312.
- Si-Mohamed SA, Boccalini S, Lacombe H, et al. Coronary CT angiography with photon-counting CT: first-in-human results. *Radiology.* 2022;303:303–313.
- Pourmorteza A, Symons R, Reich DS, et al. Photon-counting CT of the brain: in vivo human results and image-quality assessment. *AJNR Am J Neuroradiol.* 2017; 38:2257–2263.
- Symons R, Pourmorteza A, Sandfort V, et al. Feasibility of dose-reduced chest CT with photon-counting detectors: initial results in humans. *Radiology.* 2017; 285:980–989.
- Pourmorteza A, Symons R, Henning A, et al. Dose efficiency of quarter-millimeter photon-counting computed tomography: first-in-human results. *Invest Radiol.* 2018; 53:365–372.
- Leng S, Rajendran K, Gong H, et al. 150- $\mu$ m spatial resolution using photon-counting detector computed tomography technology: technical performance and first patient images. *Invest Radiol.* 2018;53:655–662.
- Blevins I. X-ray detectors for spectral photon-counting CT. In: Taguchi K, Blevins I, Iniewski K, eds. *Spectral, Photon Counting Computed Tomography: Technology and Applications.* Boca Raton, FL: CRC Press; 2020:179–191.
- Alvarez RE. Estimator for photon counting energy selective x-ray imaging with multibin pulse height analysis. *Med Phys.* 2011;38:2324–2334.

21. Boccacini S, Si-Mohamed SA, Lacombe H, et al. First in-human results of computed tomography angiography for coronary stent assessment with a spectral photon counting computed tomography. *Invest Radiol*. 2022;57:212–221.
22. van der Werf NR, Si-Mohamed S, Rodesch PA, et al. Coronary calcium scoring potential of large field-of-view spectral photon-counting CT: a phantom study. *Eur Radiol*. 2022;32:152–162.
23. Si-Mohamed SA, Greffier J, Miaillhes J, et al. Comparison of image quality between spectral photon-counting CT and dual-layer CT for the evaluation of lung nodules: a phantom study. *Eur Radiol*. 2021;32:524–532.
24. Kopp FK, Daerr H, Si-Mohamed S, et al. Evaluation of a preclinical photon-counting CT prototype for pulmonary imaging. *Sci Rep*. 2018;8:17386.
25. van der Werf NR, Rodesch PA, Si-Mohamed S, et al. Improved coronary calcium detection and quantification with low-dose full field-of-view photon-counting CT: a phantom study. *Eur Radiol*. 2022;32:3447–3457.
26. Greffier J, Si-Mohamed SA, Lacombe H, et al. Virtual monochromatic images for coronary artery imaging with a spectral photon-counting CT in comparison to dual-layer CT systems: a phantom and preliminary human study. *Eur Radiol*. 2023.
27. Boccacini S, Si-Mohamed S, Dessouky R, et al. Feasibility of human vascular imaging of the neck with a large field-of-view spectral photon-counting CT system. *Diagn Interv Imaging*. 2021;102:329–332.
28. Bartlett DJ, Koo CW, Bartholmai BJ, et al. High-resolution chest computed tomography imaging of the lungs: impact of 1024 matrix reconstruction and photon-counting detector computed tomography. *Invest Radiol*. 2019;54:129–137.
29. Greffier J, Frandon J. Spectral photon-counting CT system: toward improved image quality performance in conventional and spectral CT imaging. *Diagn Interv Imaging*. 2021;102:271–272.
30. Zhou W, Montoya J, Gutjahr R, et al. Lung nodule volume quantification and shape differentiation with an ultra-high resolution technique on a photon counting detector CT system. *Proc SPIE Int Soc Opt Eng*. 2017;10132:101323Q.
31. Gao F, Li M, Ge X, et al. Multi-detector spiral CT study of the relationships between pulmonary ground-glass nodules and blood vessels. *Eur Radiol*. 2013;23:3271–3277.
32. Gao F, Sun Y, Zhang G, et al. CT characterization of different pathological types of subcentimeter pulmonary ground-glass nodular lesions. *Br J Radiol*. 2019;92:20180204.
33. Inoue A, Johnson TF, White D, et al. Estimating the clinical impact of photon-counting-detector CT in diagnosing usual interstitial pneumonia. *Invest Radiol*. 2022;57:734–741.
34. Lynch DA, Sverzellati N, Travis WD, et al. Diagnostic criteria for idiopathic pulmonary fibrosis: a Fleischner Society white paper. *Lancet Respir Med*. 2018;6:138–153.
35. Si-Mohamed SA, Nasser M, Colevray M, et al. Automatic quantitative computed tomography measurement of longitudinal lung volume loss in interstitial lung diseases. *Eur Radiol*. 2022;32:4292–4303.
36. Si-Mohamed SA, Miaillhes J, Rodesch P-A, et al. Spectral photon-counting CT technology in chest imaging. *J Clin Med*. 2021;10:5757.
37. Han MK, Kazerooni EA, Lynch DA, et al. Chronic obstructive pulmonary disease exacerbations in the COPDGene study: associated radiologic phenotypes. *Radiology*. 2011;261:274–282.
38. Knuuti J, Wijns W, Saraste A, et al. 2019 ESC guidelines for the diagnosis and management of chronic coronary syndromes. *Eur Heart J*. 2020;41:407–477.
39. Seitun S, Castiglione Morelli M, Budaj I, et al. Stress computed tomography myocardial perfusion imaging: a new topic in cardiology. *Rev Esp Cardiol Engl Ed*. 2016;69:188–200.
40. Boussel L, Ribagnac M, Bonnefoy E, et al. Assessment of acute myocardial infarction using MDCT after percutaneous coronary intervention: comparison with MRI. *Am J Roentgenol*. 2008;191:441–447.
41. Otto CM, Nishimura RA, Bonow RO, et al. 2020 ACC/AHA guideline for the management of patients with valvular heart disease: a report of the American College of Cardiology/American Heart Association Joint Committee on Clinical Practice Guidelines. *Circulation*. 2021;143:e72–e227.
42. Francone M, Budde RPJ, Bremerich J, et al. CT and MR imaging prior to transcatheter aortic valve implantation: standardization of scanning protocols, measurements and reporting—a consensus document by the European Society of Cardiovascular Radiology (ESCR). *Eur Radiol*. 2020;30:2627–2650.
43. Sandstedt M, Marsh J Jr, Rajendran K, et al. Improved coronary calcification quantification using photon-counting-detector CT: an ex vivo study in cadaveric specimens. *Eur Radiol*. 2021;31:6621–6630.
44. Sigovan M, Si-Mohamed S, Bar-Ness D, et al. Feasibility of improving vascular imaging in the presence of metallic stents using spectral photon counting CT and K-edge imaging. *Sci Rep*. 2019;9:19850.
45. Rotzinger D, Racine D, Becce F, et al. Performance of spectral photon-counting coronary CT angiography and comparison with energy-integrating-detector CT: objective assessment with model observer. *Diagnostics (Basel)*. 2021;11:2376. <https://pubmed.ncbi.nlm.nih.gov/34943611/>. Accessed January 4, 2022.
46. Mergen V, Eberhard M, Manka R, et al. First in-human quantitative plaque characterization with ultra-high resolution coronary photon-counting CT angiography. *Front Cardiovasc Med*. 2022;9:981012.
47. Boussel L, Coulon P, Thran A, et al. Photon counting spectral CT component analysis of coronary artery atherosclerotic plaque samples. *Br J Radiol*. 2014;87:20130798.
48. Symons R, Sandfort V, Mallek M, et al. Coronary artery calcium scoring with photon-counting CT: first in vivo human experience. *Int J Cardiovasc Imaging*. 2019;35:733–739.
49. Symons R, Reich DS, Bagheri M, et al. Photon-counting computed tomography for vascular imaging of the head and neck. *Invest Radiol*. 2018;53:135–142.
50. Wehrle E, Sawall S, Klein L, et al. Potential of ultra-high-resolution photon-counting CT of bone metastases: initial experiences in breast cancer patients. *Npj Breast Cancer*. 2021;7:3.
51. Baffour FI, Huber NR, Ferrero A, et al. Photon-counting detector CT with deep learning noise reduction to detect multiple myeloma. *Radiology*. 2023;306:229–236.
52. Chappard C, Abascal J, Olivier C, et al. Virtual monoenergetic images from photon-counting spectral computed tomography to assess knee osteoarthritis. *Eur Radiol Exp*. 2022;6:10.
53. Benson JC, Rajendran K, Lane JI, et al. A new frontier in temporal bone imaging: photon-counting detector CT demonstrates superior visualization of critical anatomic structures at reduced radiation dose. *Am J Neuroradiol*. 2022;43:579–584.
54. Jungblut L, Euler A, von Spiczak J, et al. Potential of photon-counting detector CT for radiation dose reduction for the assessment of interstitial lung disease in patients with systemic sclerosis. *Invest Radiol*. 2022;57:773–779.
55. Boccacini S, Si-Mohamed S, Matzuzzi M, et al. Effect of contrast material injection protocol on first-pass myocardial perfusion assessed by dual-energy dual-layer computed tomography. *Quant Imaging Med Surg*. 2022;12:3903–3916.
56. Jungblut L, Abel F, Nakhostin D, et al. Impact of photon-counting-detector-CT derived virtual-monoenergetic-images and iodine-maps on the diagnosis of pleural empyema [published online ahead of print October 7, 2022]. *Diagn Interv Imaging*. S2211-5684(22)00187-5.
57. Rotzinger DC, Si-Mohamed SA, Yerly J, et al. Reduced-iodine-dose dual-energy coronary CT angiography: qualitative and quantitative comparison between virtual monochromatic and polychromatic CT images. *Eur Radiol*. 2021;31:7132–7142.
58. Leithner D, Wichmann JL, Vogl TJ, et al. Virtual monoenergetic imaging and iodine perfusion maps improve diagnostic accuracy of dual-energy computed tomography pulmonary angiography with suboptimal contrast attenuation. *Invest Radiol*. 2017;52:659–665.
59. Emrich T, O'Doherty J, Schoepf UJ, et al. Reduced iodinated contrast media administration in coronary CT angiography on a clinical photon-counting detector CT system: a phantom study using a dynamic circulation model. *Invest Radiol*. 2023;58:148–155.
60. Jungblut L, Kronenberg D, Mergen V, et al. Impact of contrast enhancement and virtual monoenergetic image energy levels on emphysema quantification: experience with photon-counting detector computed tomography. *Invest Radiol*. 2022;57:359–365.
61. Bratke G, Hicketier T, Bar-Ness D, et al. Spectral photon-counting computed tomography for coronary stent imaging: evaluation of the potential clinical impact for the delineation of in-stent restenosis. *Invest Radiol*. 2020;55:61–67.
62. Khodarahmi I, Haroun RR, Lee M, et al. Metal artifact reduction computed tomography of arthroplasty implants: effects of combined modeled iterative reconstruction and dual-energy virtual monoenergetic extrapolation at higher photon energies. *Invest Radiol*. 2018;53:728–735.
63. Si-Mohamed S, Moreau-Triby C, Tyłski P, et al. Head-to-head comparison of lung perfusion with dual-energy CT and SPECT-CT. *Diagn Interv Imaging*. 2020;101:299–310.
64. Si-Mohamed S, Bar-Ness D, Sigovan M, et al. Multicolour imaging with spectral photon-counting CT: a phantom study. *Eur Radiol Exp*. 2018;2:34.
65. Cormode DP, Si-Mohamed S, Bar-Ness D, et al. Multicolor spectral photon-counting computed tomography: in vivo dual contrast imaging with a high count rate scanner. *Sci Rep*. 2017;7:4784.
66. Si-Mohamed S, Thivolet A, Bonnot P-E, et al. Improved peritoneal cavity and abdominal organ imaging using a biphasic contrast agent protocol and spectral photon counting computed tomography K-edge imaging. *Invest Radiol*. 2018;53:629–639.
67. Si-Mohamed S, Cormode DP, Bar-Ness D, et al. Evaluation of spectral photon counting computed tomography K-edge imaging for determination of gold nanoparticle biodistribution in vivo. *Nanoscale*. 2017;9:18246–18257.
68. Cuccione E, Chhour P, Si-Mohamed S, et al. Multicolor spectral photon counting CT monitors and quantifies therapeutic cells and their encapsulating scaffold in a model of brain damage. *Nanotheranostics*. 2020;4:129–141.

69. Kim J, Bar-Ness D, Si-Mohamed S, et al. Assessment of candidate elements for development of spectral photon-counting CT specific contrast agents. *Sci Rep.* 2018;8:12119.
70. Si-Mohamed SA, Sigovan M, Hsu JC, et al. In vivo molecular K-edge imaging of atherosclerotic plaque using photon-counting CT. *Radiology.* 2021;300:98–107.
71. Si-Mohamed S, Tatar-Leitman V, Laugerette A, et al. Spectral photon-counting computed tomography (SPCCT): in-vivo single-acquisition multi-phase liver imaging with a dual contrast agent protocol. *Sci Rep.* 2019;9:8458.
72. Dangelmaier J, Bar-Ness D, Daerr H, et al. Experimental feasibility of spectral photon-counting computed tomography with two contrast agents for the detection of endoleaks following endovascular aortic repair. *Eur Radiol.* 2018;28:3318–3325.
73. Riederer I, Bar-Ness D, Kimm MA, et al. Liquid embolic agents in spectral x-ray photon-counting computed tomography using tantalum K-edge imaging. *Sci Rep.* 2019;9:5268.
74. Halttunen N, Lerouge F, Chaput F, et al. Hybrid Nano-GdF3 contrast media allows pre-clinical in vivo element-specific K-edge imaging and quantification. *Sci Rep.* 2019;9:12090.
75. Dong YC, Kumar A, Rosario-Berrios DN, et al. Ytterbium nanoparticle contrast agents for conventional and spectral photon-counting CT and their applications for hydrogel imaging. *ACS Appl Mater Interfaces.* 2022;14:39274–39284.
76. Dong YC, Hajfathalian M, Maidment PSN, et al. Effect of gold nanoparticle size on their properties as contrast agents for computed tomography. *Sci Rep.* 2019;9:14912.
77. Naha PC, Hsu JC, Kim J, et al. Dextran-coated cerium oxide nanoparticles: a computed tomography contrast agent for imaging the gastrointestinal tract and inflammatory bowel disease. *ACS Nano.* 2020;14:10187–10197.
78. Pan D, Schirra CO, Senpan A, et al. An early investigation of ytterbium nanocolloids for selective and quantitative “multicolor” spectral CT imaging. *ACS Nano.* 2012;6:3364–3370.
79. Cormode DP, Roessl E, Thran A, et al. Atherosclerotic plaque composition: analysis with multicolor CT and targeted gold nanoparticles. *Radiology.* 2010;256:774–782.
80. Thivolet A, Si-Mohamed S, Bonnot P-E, et al. Spectral photon-counting CT imaging of colorectal peritoneal metastases: initial experience in rats. *Sci Rep.* 2020;10:13394.
81. de Vries A, Roessl E, Kneepkens E, et al. Quantitative spectral K-edge imaging in preclinical photon-counting x-ray computed tomography. *Invest Radiol.* 2015;50:297–304.
82. Cosset B, Sigovan M, Boccalini S, et al. Bicolor K-edge spectral photon-counting CT imaging for the diagnosis of thoracic endoleaks: a dynamic phantom study [published online ahead of print January 15, 2023]. *Diagn Interv Imaging.*